# Grooved Nanowires from Self-Assembling Hairpin Molecules for Solar Cells

**Ian D. Tevis,[†,∥] Wei-Wen Tsai,[†,∥] Liam C. Palmer,[†] Taner Aytun,[‡] and Samuel I. Stupp[†,‡,§,⊥,*]**

[†]Department of Chemistry, [‡]Department of Materials Science and Engineering and [§]Medicine, and [⊥]Institute for BioNanotechnology in Medicine, Northwestern University, 2220 Campus Drive, Evanston, Illinois 60208, United States. [∥]These authors contributed equally to this work.

**ABSTRACT**

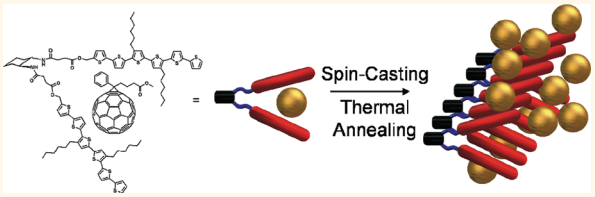


One of the challenges facing bulk heterojunction organic solar cells is obtaining organized films during the phase separation of intimately mixed donor and acceptor components. We report here on the use of hairpin-shaped sexithiophene molecules to generate by self-assembly grooved nanowires as the donor component in bulk heterojunction solar cells. Photovoltaic devices were fabricated *via* spin-casting to produce by solvent evaporation a percolating network of self-assembled nanowires and fullerene acceptors. Thermal annealing was found to increase power conversion efficiencies by promoting domain growth while still maintaining this percolating network of nanostructures. The benefits of self-assembly and grooved nanowires were examined by building devices from a soluble sexithiophene derivative that does not form one-dimensional structures. In these systems, excessive phase separation caused by thermal annealing leads to the formation of defects and lower device efficiencies. We propose that the unique hairpin shape of the self-assembling molecules allows the nanowires as they form to interact well with the fullerenes in receptor–ligand type configurations at the heterojunction of the two domains, thus enhancing device efficiencies by 23%.

**KEYWORDS:** self-assembly · organogelator · sexithiophene · nanowire · photovoltaic · morphology

Organic bulk heterojunction photovoltaics have received much attention in recent years because of their potential to produce low-cost solar energy.[1] Donor molecules like poly(3-hexylthiophene) (P3HT) and acceptor molecules like phenyl-$C_{61}$-butyric acid methyl ester (PCBM) have been at the forefront of this field with moderate single-digit power conversion efficiencies.[2−6] Such polymers and small molecules can be intimately mixed on the nanoscale in approximately a 50:50 weight ratio and spin-cast onto transparent conducting electrodes to form bulk heterojunction solar cells. In organic solar cells, light absorption creates excitons (bound electron−hole pairs) and not free carriers. Intimate mixing keeps the donor and acceptor molecules in close proximity, which assists in the spliting of excitons into electrons and holes before their recombination.[5] Transporting these carriers through the mixture is dependent on the crystallinity of the two components and their nanoscale morphology.[7] Controlling the phase separation and crystalline growth depends strongly on drying conditions, annealing conditions, the propensity of molecules to crystallize individually in the mixtures, and the bulkiness of side groups.[1,8] Some control over crystallinity and morphology of the mixture has been be accomplished by selecting solvents with different vapor pressures. Solvents with lower vapor pressures dry at a slower rate, and this allows the two components of the spin-cast film to crystallize together while the film dries.[9−12] Ideally, controlling these variables creates interspersed domains of ordered semiconductors that allow efficient exciton splitting and charge transport. Recently, small molecules have been successfully used in place of donating polymers using very similar stratagies to obtain interspersed domains of donors and acceptors.[13−17] The best of these linear small molecules reported by us and others have reached power conversion efficiencies (PCE) over 4%.[13,18] Small molecules have advantages over polymers such as synthetic versatility, higher carrier mobilities, straightforward purification and possibly recycling, and the potential to create more monodisperse structures. However, even with small molecules, it remains difficult to control the phase separation or the directionality of the growing domains.

* Address correspondence to s-stupp@northwestern.edu.

Received for review August 29, 2011 and accepted February 9, 2012.

**Published online March 07, 2012**
**10.1021/nn203328n**

Hydrogen bonding, $\pi-\pi$ stacking, and evaporation-induced self-assembly have been used by us and others to control organization on the molecular level to construct molecules into larger supramolecular structures.[19−48] The first published example to directly use a semiconducting organogelator as an active material in a bulk heterojunction system reached a power conversion efficiency of 0.04%.[49] This example utilized a linear organogelator to form coarse films of bundled fibers blended in an amorphous polymer. The ability to control the specific shapes of 1D supramolecular assemblies through molecular design offers the possibility of fine-tuning their functions. In an earlier example, we showed the possibility of forming mirror image helical wires using two different enantiomers,[50] and recently, we reported on 1D assemblies of a hairpin-shaped oligothiophene with the purpose of forming "grooved" wires for complexation with other molecules.[51] The hairpin molecules were found to assemble spontaneously into one-dimensional (1D) nanowires driven by both $\pi-\pi$ stacking and hydrogen bonding.[51] At concentrations greater than 0.5 wt %, long nanowires formed and interpenetrated creating a self-supporting gel in toluene and chlorocyclohexane. We found evidence of their grooved nature in their distinct ability to form both H-aggregated $\pi-\pi$ stacks along the principal axis of the nanowire as well as J-aggregates, which must originate in bundling due to edge-to-edge interactions among arms of the hairpin molecules. The presence of both H- and J-aggregates was found to broaden light absorption due to blue (H) and red shifts (J) and should also facilitate charge transport along the nanowire as well as between nanowires. We report here the incorporation of the hairpin-shaped self-assembling semiconducting oligothiophene described above into bulk heterojunction devices with small molecule fullerene acceptors. In contrast to linear molecules, the grooved nature of the wires formed by hairpin-shaped molecules should enhance interfacial contact between donor and acceptor components. Photovoltaic devices were characterized by current density−voltage and external quantum efficiency meausurements, and film morphology was probed by atomic force microscopy.

## RESULTS AND DISCUSSION

Assemblies of the hairpin-shaped sexithiophene molecule (M1, Figure 1) have been determined to be p-type semiconducting with HOMO and LUMO levels[51] well positioned relative to PCBM (see Figure 1) to be an efficient electron donor (Figure 2). One characteristic of energy transfer between donor and acceptor molecules is fluorescence quenching of the donor chromophores. A fluorescence titration study was performed on M1 in toluene and chlorobenzene in order to assess the different quenching processes of the assembled and nonassembled states, respectively.

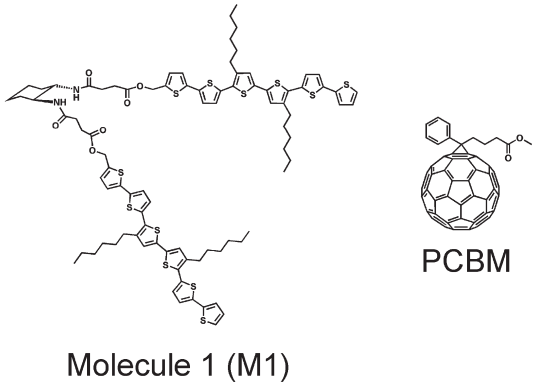


**Figure 1. Molecular structure of hairpin-shaped sexithiophene molecule (M1) used as the hole-transporting p-type semiconductor in the bulk heterojunction photovoltaic devices. The n-type semiconductors, PCBM, used as the acceptor and electron-transporting component.**

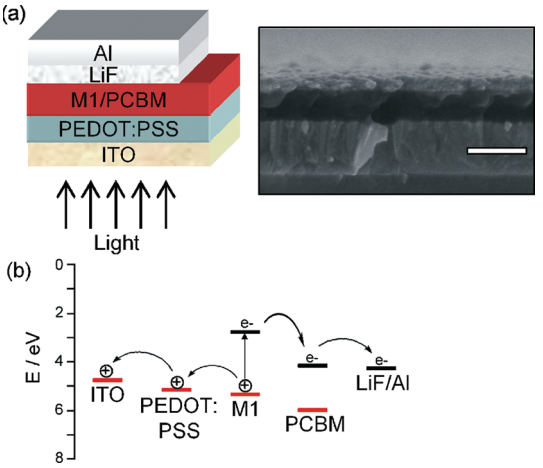


**Figure 2. (a) Schematic representation of the photovoltaic device and scanning electron microscopy (SEM) image (right) of a cross section of the device. Scale bar is 100 nm. (b) Energy diagram showing HOMO and LUMO levels of M1 and PCBM with the work functions of both electrodes and the route of carrier transport.**

M1 readily aggregates in toluene but does not form self-assembled nanostructures in chlorobenzene. Figure S1 (Supporting Information) shows the fluorescence spectra of M1 in toluene in response to the titration of PCBM. The fluorescence of M1 is significantly attenuated with increasing PCBM concentration, eventually leading to a 78% quenching of the intensity. This result strengthens our assumption that the fluorescence quenching is the result of efficient energy transfer from the excited sexithiophene moieties to ground-state PCBM molecules. A more detailed analysis can be found in the Supporting Information.

Photovoltaic devices (see Figure 2) were fabricated from blends of M1 and PCBM in chlorobenzene at various weight ratios in order to ascertain the optimal ratio (Figure S2). It was determined that a M1/PCBM weight ratio of 40:60 gave the highest efficiency, and all subsequent devices were fabricated from this

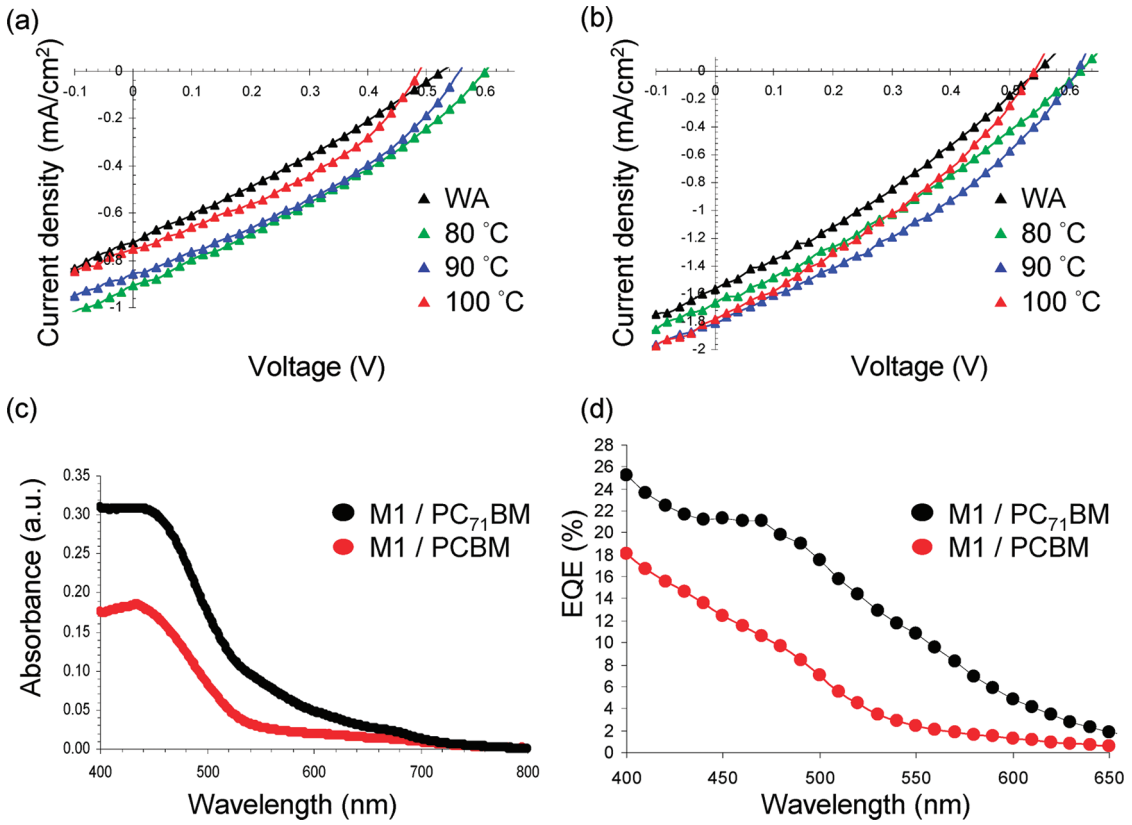


**Figure 3. (a) *J*–*V* curves from M1/PCBM devices before and after thermal annealing at different temperatures. (b) Photovoltaic *J*–*V* curves from M1/$PC_{71}BM$ blend before and after thermal annealing at different temperatures. (c) UV–vis spectra of thin-film devices showing additive absorption of the fullerenes and H-aggregated M1. (d) External quantum efficiency (EQE) of the device.**

optimized composition. During fabrication of all devices, the active layer dries during spin-coating, which effectively holds the two components in place. On the nanoscale, these components are intimately mixed, which benefits exciton splitting, but fast drying can lead to partially disordered domains that can compromise charge transport. Large spatial overlap assists charge hopping by shortening intermolecular distances, but disorder decreases spatial overlap of $\pi$-orbitals between adjacent molecules, scattering carriers as they are transported and leading to lower short-circuit current densities ($J_{sc}$).[52] Current density (*J*) *versus* voltage (*V*) plots of illuminated devices without annealing (WA) demonstrated a PCE of 0.14% with a $J_{sc}$ of 0.72 mA/cm$^2$ (Figure 3a and Table 1).

Typically, bulk heterojunction solar cells are thermally annealed after the cast films dry or after metal evaporation in order to increase device efficiency.[2,53–55] Annealing allows the two components to phase separate, crystallize, and form intermixed ordered domains facilitating charge transport while maintaining a high exciton splitting efficiency. M1/PCBM devices were annealed in a glovebox for 2 min at various temperatures up to 100 °C (see Figure 3a and Table 1). Annealing at 80 °C increased the $J_{sc}$ to 0.91 mA/cm$^2$ as well as the open-circuit voltage ($V_{oc}$) from 0.53 to 0.61 V.

**TABLE 1. Photovoltaic Characteristics of 40:60 Blends of M1/PCBM Annealed at Various Temperatures**

| annealing conditions | $J_{sc}$ (mA/cm$^2$) | $V_{oc}$ (V) | FF (%) | $\eta$ (%) |
|---|---|---|---|---|
| without annealing | 0.72 | 0.53 | 29 | 0.14 |
| 80 °C | 0.91 | 0.61 | 32 | 0.22 |
| 90 °C | 0.86 | 0.56 | 35 | 0.21 |
| 100 °C | 0.76 | 0.49 | 37 | 0.17 |

Additional annealing at 90 °C had a negative effect on the $V_{oc}$, decreasing it to 0.56 V. Annealing at this temperature also decreased the $J_{sc}$ to 0.86 mA/cm$^2$ but increased the fill factor (FF) to 35%. This increase in FF was enough to offset the decreased $J_{sc}$ and $V_{oc}$, leading to a 0.21% efficient device. Further annealing at 100 °C caused decreases of $J_{sc}$ to 0.76 mA/cm$^2$, $V_{oc}$ to 0.49 V, but an increase in FF to 37%. The best annealing conditions were at 80 °C, yielding an overall efficiency of 0.22%, which is over 57% higher than the devices without annealing.

Pure M1 has a solid-state melting transition starting at approximately 100 °C and peaking at 109 °C as measured by differential scanning calorimetry (DSC) (Figure S3). Optical microscopy through crossed polars of drop-cast films demonstrated birefringence, which is an indication of anisotropy, most likely from the 1D structures. Birefringence was lost upon heating to

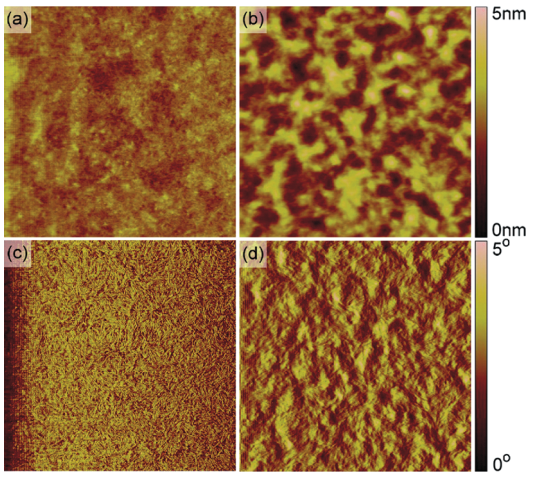


**Figure 4. AFM topography (top) and phase (bottom) images of a M1/PCBM film. (a,c) Before thermal annealing and (b,d) after thermal annealing. The nonannealed film has a roughness of $R_a$ = 1.12 nm, whereas the annealed film has a $R_a$ of 2.35 nm due to domain growth. Each graph is 2 $\mu$m × 2 $\mu$m.**

109 °C and was not regained when cooled, suggesting that the self-assembled structures melt at this temperature and do not reassemble upon cooling. In bulk heterojunction solar cells, thermal annealing facilitates phase separation in the solid state and the crystallization of each component, both of which promote better charge carrier transport and minimized charge trapping.[56] The peak efficiencies of M1/PCBM devices were observed for annealing temperatures of 80 and 90 °C, which are both below the observed melting transition. When we anneal devices to the start of the melting transition (100 °C), there is a decrease in efficiency because the M1 partially melts and the assembly does not re-form upon cooling. Irreversible loss of the self-assembled nanostructures of M1 is accompanied by a drop in $J_{sc}$ and $V_{oc}$.

Atomic force microscopy (AFM) was performed on M1/PCBM films before and after annealing to characterize their surface morphologies (Figure 4). AFM topographic images of the spin-cast films are very smooth, having an average surface roughness ($R_a$) of only 1.12 nm. We observed small, dispersed, fiber-like structures in the topography and phase images, which suggest that during drying M1 phase separates from the PCBM and assembles into nanowires (see Figure 4a,c and Figure S4 for enlarged Figure 4c). These nanowires formed by evaporation-induced self-assembly dry quickly and presumably trap the PCBM in a percolating network based on our observation of photovoltaic activity in the devices prepared. When the devices are annealed the surface roughness ($R_a$) increases to 2.35 nm, which can be an indicator of an increase in domain sizes.[13] We believe that the addition of thermal energy assists further assembly of M1 and the aggregation of the PCBM, causing the growth of nanoscale domains. When the films are annealed, M1 fibers can grow longer and interconnect but still allow the PCBM to crystallize and remain intimately mixed with M1. Specifically, the hydrogen-bonding groups and $\pi-\pi$ stacking moieties of M1 synergistically guide assembly and domain growth while maintaining the interpenetrating network of nanowires in the solid film, which should facilitate charge transport while maintaining a high exciton splitting efficiency. These thermally induced morphological changes are not accompanied by any change in absorbance (Figure S5). Space-charge-limited current measurements[57] were performed in order to determine the effect of thermal annealing on the hole transporting properties of M1 in a blended film of M1/PCBM. A detailed description of these experiments can found in the Supporting Information. Upon thermal annealing at 80 °C, hole mobility was found to increase from 4.1 × $10^{-10}$ to 6.5 × $10^{-10}$ $m^2/V \cdot s$ and $J_{sc}$ was found to increase as well (Figure S6 and Table S1). Further annealing at 90 °C significantly decreased the hole mobility to 2.7 × $10^{-10}$ $m^2/V \cdot s$, while the $J_{sc}$ was observed to be higher than that in devices that were not annealed. These observed changes in $J_{sc}$ are not caused by an increase in light absorption and cannot be entirely explained by an increase in hole mobility. The observed increase in $J_{sc}$ could also be caused by an increase in exciton splitting efficiency.

It is clear that evaporation-induced self-assembly in films cast from chlorobenzene generates an efficient nanoscale morphology, but it may be possible to improve this morphology without assistance from annealing. Utilizing solvents to preform nanowires in solution could improve charge transport by extending the length of nanowires while still maintaining intimate mixing with PCBM. M1 assembles in toluene but not in chlorobenzene, and by changing the solvent to toluene, M1 is known to form aggregates in solution.[51] When M1/PCBM blends are spin-cast from toluene, the dried film should exhibit the same interpenetrating network of nanostructures observed in films cast from chlorobenzene but with longer and more interconnected domains of assembled M1. The resulting films cast from toluene had a high surface roughness and some gaps leading to photovoltaic devices with low $J_{sc}$ and low $V_{oc}$ (Figure S7). During drying, the preassembled M1 structures extended and interpenetrated to the point that weak gelation occurred. This limits the amount of interfacial contact between M1 and PCBM and creates coarse areas of macroscopic aggregates. Exciton splitting efficiencies in these films are suspected to be low, and devices made from these preaggreagated blends exhibited lower $J_{sc}$. Coarse films lead to a significant number of gaps creating areas for potential shorting between the Al and PEDOT:PSS contacts during thermal evaporation, which can lower the $V_{oc}$. This aggregation has been observed with other organogelator bulk

**TABLE 2. Photovoltaic Characteristics of 40:60 Blends of M1/$PC_{71}BM$ Annealed at Various Temperatures**

| annealing conditions | $J_{sc}$ (mA/cm$^2$) | $V_{oc}$ (V) | FF (%) | $\eta$ (%) |
|---|---|---|---|---|
| without annealing | 1.54 | 0.55 | 31 | 0.33 |
| 80 °C | 1.66 | 0.62 | 32 | 0.41 |
| 90 °C | 1.79 | 0.62 | 35 | 0.48 |
| 100 °C | 1.78 | 0.55 | 33 | 0.40 |

heterojunction systems.[49] By comparing assembling and nonassembling solvents, we conclude that evaporation-induced self-assembly is more effective than utilizing preassembled nanostructures at producing the smoothest and most efficient nanoscale morphology.

Exciton splitting and charge transport can be tuned by the nanoscale morphology but only contribute to part of the total PCE; light absorption is also key to higher efficiencies. PCBM has limited light absorption in the visible spectrum because symmetry of the spherical $C_{60}$ forbids low-energy transitions. The less symmetric and more ellipsoidal-shaped $C_{70}$ allows low-energy transitions and consequently greater absorption of visible light. Thus, we fabricated M1 devices with phenyl-$C_{71}$-butyric acid methyl ester ($PC_{71}BM$) in place of the PCBM following the same processing procedures described above. M1/$PC_{71}BM$ devices measured without annealing have $J-V$ curves with identical shapes to the M1/PCBM devices but have a larger $J_{sc}$ of 1.54 mA/cm$^2$ leading to an efficiency of 0.33% (see Figure 3b and Table 2). Annealing studies were also performed on this blend, and the devices demonstrated the same trend of increased device efficiency with thermal annealing. A maximum PCE of 0.48% was reached when devices were annealed at 90 °C. This is more than twice the efficiency of devices fabricated with PCBM and 45% higher than the efficiency of unannealed devices. The larger 0.48% efficiency originates from an increase in $J_{sc}$ to 1.79 mA/cm$^2$ and FF to 35% while maintaining a $V_{oc}$ at 0.62 V. Devices demonstrated a drop in $V_{oc}$ and efficiency when annealed at 100 °C, consistent with the PCBM devices except that the optimal annealing temperature is higher. Films before and after annealing demonstrate similar topography as those containing PCBM (Figure S8). The melting point of $PC_{71}BM$ (321 °C) is significantly higher than for PCBM (290 °C);[58] this melting point difference may explain the lower impact of thermal annealing and the higher maximum annealing temperature. The observed efficiency of 0.48% is over an order of magnitude higher than previously published organogelator-based bulk heterojunction devices (note: devices reported by Wicklein *et al.* were measured under an intensity of 100 mW/cm$^2$).[49]

UV–vis absorption spectra were collected for films of M1/PCBM and M1/$PC_{71}BM$ after annealing (see Figure 3c). The larger light absorption of $PC_{71}BM$-based films *versus* PCBM was evident and is likely the largest source of the increase in $J_{sc}$. The absorption of M1 combined with the absorption of the PCBM and $PC_{71}BM$ leads to a $\lambda_{max}$ of 430 and 439 nm, respectively. The UV–visible spectroscopy (UV–vis) spectra are compared in Figure 3c,d to external quantum efficiency (EQE) data collected for the devices at their best annealing conditions. In the $PC_{71}BM$ devices, a shoulder peak was observed at 471 nm that is attributed to the absorption of $PC_{71}BM$. The EQE of the blended films is broad between 400 and 600 nm and extends into the UV region.

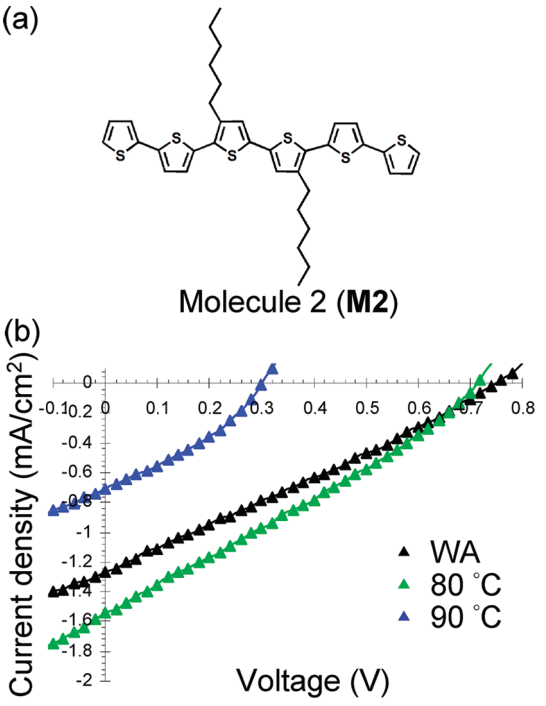


**Figure 5. (a) Dihexylsexithiophene (M2) used as a control. (b) Photovoltaic $J-V$ curves of a ratio of 40:60 M2/$PC_{71}BM$ annealed at different temperatures.**

**TABLE 3. Photovoltaic Characteristics of 40:60 Blends of M2/$PC_{71}BM$ Annealed at Various Temperatures**

| annealing conditions | $J_{sc}$ (mA/cm$^2$) | $V_{oc}$ (V) | FF (%) | $\eta$ (%) |
|---|---|---|---|---|
| without annealing | 1.23 | 0.75 | 26 | 0.32 |
| 80 °C | 1.55 | 0.71 | 28 | 0.39 |
| 90 °C | 0.70 | 0.30 | 35 | 0.09 |
| 90 °C again | 0.54 | 0.21 | 36 | 0.05 |

In order to better understand the role of self-assembly in this system, we fabricated devices based on a dihexylsexithiophene (M2, Figure 5), which has the same oligothiophene moiety but with linear rather than hairpin architecture and also lacks hydrogen-bonding motifs. Devices were fabricated from identical conditions to those described previously for the M1/$PC_{71}BM$ devices processed from chlorobenzene. Photovoltaic curves from these devices before and after

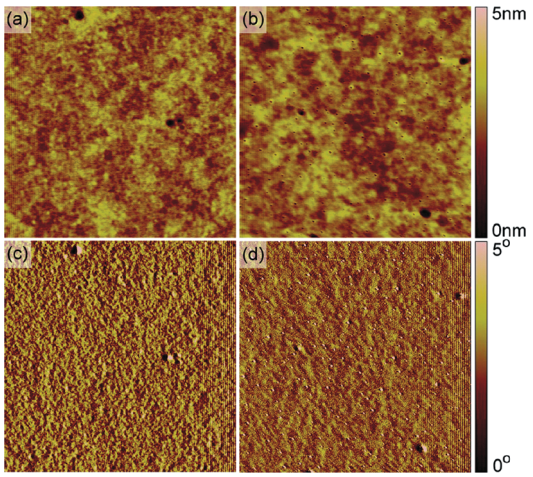


**Figure 6. AFM topography (top) and phase (bottom) images of M2/$PC_{71}BM$ films (a,c) before thermal annealing and (b,d) after thermal annealing. The nonannealed film has a $R_a$ of 0.426 nm, whereas the annealed film has an average $R_a$ of 0.377 nm. The scan size for all images is 2 $\mu$m × 2 $\mu$m.**

annealing are shown in Figure 5, and the results are summarized in Table 3. The efficiency of the devices measured before annealing was 0.32%, which is nearly identical to the M1/$PC_{71}BM$ devices. Annealing the devices at 80 °C increased the $J_{sc}$ from 1.23 to 1.55 mA/cm$^2$ but decreased the $V_{oc}$ from 0.75 to 0.71 V, resulting in a PCE of 0.39%. This observed $J_{sc}$ is identical to the $J_{sc}$ of M1/$PC_{71}BM$ devices without annealing (see Table 2). Annealing these devices at 90 °C dramatically decreased the PCE to 0.09% because of a large drop in both $J_{sc}$ and $V_{oc}$; additional annealing at 90 °C caused the device to degrade further to 0.05%.

UV−vis absorption spectra of the M2 devices were collected before and after annealing (Figure S9). The $\lambda_{max}$ of the film without annealing is observed at approximately 450 nm with a blue shift to 430 nm upon annealing at 80 °C. There was little change in the spectrum after annealing at higher temperatures. This blue shift observed after annealing is an indication of H-aggregation among M2 molecules. Optical changes have been observed in bulk heterojunction systems as a result of increased organization and improved nanoscale morphology usually accompanied by an increase in efficiency.[53] On the other hand, films of the M2/$PC_{71}BM$ blend show no discernible nanostructure by AFM (Figure 6). Even upon annealing when optical changes were observed, there is no discernible nanostructure observed. However, annealing does cause the appearance of nanoscale defects in the film. We attribute these holes to extensive phase separation of the two components, which explains the drastic efficiency decrease observed when films are annealed above 80 °C.

When M1 gels in toluene, it is an indication that toluene is trapped within a three-dimensional scaffold of nanowires. We believe the same structure can develop from evaporation-induced self-assembly of blends of M1 and PCBM from chlorobenzene, as the solvent evaporates and the PCBM is trapped in a network of nanostructures, as seen in the AFM topography and phase images of M1/PCBM blends (see Figure 4c). Even though there may not be long nanowires on the surface, the aggregation of M1 prevents extensive phase separation and aggregation of the PCBM. M2 does not form nanowires and thus does not have the capacity to trap PCBM in this manner, allowing large phase separation and heterogeneous aggregation that leads to defect formation in device films.

M1 was designed to pack in a specific way controlled by $\pi-\pi$ stacking and hydrogen bonding to form 1D nanostructures. We propose here that the unique hairpin-shaped structure of M1 leads to supramolecular nanowires that can contain grooves along their principal axes (Figure 7). It has been observed previously that M1 nanowires can bundle and their $\pi-\pi$ stacked sexithiophene arms can interdigitate and interact edge-to-edge within these grooves forming J-aggregates. Packing of hairpin-shaped structures into J-aggregates in solution was only observed after several days.[51] The hairpin shape hinders the packing of M1, and when a solution of M1 is dried rapidly during spin-casting, J-aggregation is not observed (Figure S10). This frustrated packing leaves a film with void space in the grooves of the nanostructure. At the molecular level, the arms of the hairpin structure are sufficiently flexible to allow the inclusion of small molecules like PCBM. Small molecules with similar shapes and noncovalent interactions have been shown to complex with fullerenes in a similar way.[59,60] We believe that, at the interface between the assembled M1 phase and the PCBM phase, some PCBM molecules can fill the grooves of M1 upon drying. M1 can then effectively form cavities in the aggregated state to host PCBM molecules at the interfacial heterojunction while the film is drying, and this interfacial organization can be preserved during the annealing process. We explained above that the increases in efficiency cannot be fully explained by changes in hole mobility and or light absorption. A thermally induced increase in $J_{sc}$ could be caused by an improvement of the quality of the interface between assembled M1 and aggregated PCBM, resulting in more efficient exciton splitting. We hypothesize here that the grooved shape of M1 nanowires allows for better complexation with PCBM, thus preventing excessive phase separation and promoting higher quality interfaces for exciton splitting. The linear M2 lacks this shape-based complexation provided by a hairpin cross section of the nanowires, thus preventing formation of nanoscale structures upon annealing that are more suited for charge separation. The mean PCE of M1 was 0.42% with a standard deviation (SD) of 0.03 for 12 devices, whereas the mean PCE of M2 was 0.36% with a SD of 0.05 for 11 devices. We performed a Welch's unpaired *t* test at the 1% significance level in

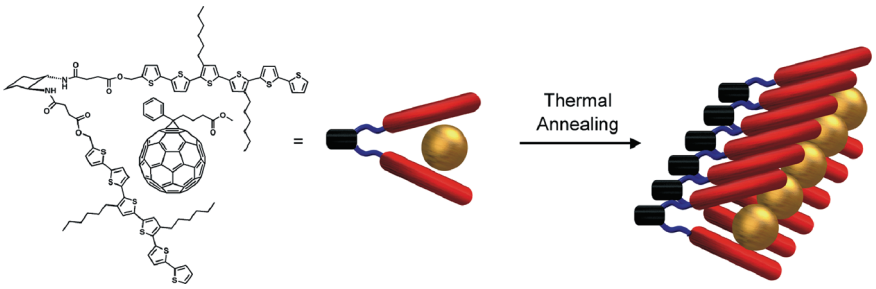


**Figure 7. Proposed nanostructural organization of M1 and PCBM molecules. The hairpin-shaped molecular geometry harbors PCBM within the self-assembled cavity of M1 and facilitates efficient exciton splitting by preventing an excessive amount of PCBM aggregation while maintaining great electron transport ability through alignment.**

order to determine if the difference in mean between M1 and M2 was significant. A two-tail $p$ value of 0.0007 was obtained, and at the 1% significance level, the data do provide sufficient evidence to conclude that the difference in power conversion efficiencies of M1 and M2 is statistically significant.

## CONCLUSIONS

We have investigated the use of self-assembly hairpin molecules as the donor component of solar cell devices. These molecules were found to make nanowires in the presence of PCBM and gave more efficient devices than those made with linear molecules. The unique hairpin shape was designed to create grooved nanowires that could enhance interfacial interaction with fullerene acceptor molecules. This grooved structure could promote receptor–ligand type configurations in bulk heterojunctions and improve device efficiency after annealing creates percolating domains for charge transport.

## EXPERIMENTAL METHODS

**General.** All chemicals were purchased from commercial sources (Sigma-Aldrich, Nano-C, or H.C. Starck) and used without further purification unless otherwise noted. Solvents (chlorobenzene and toluene) were distilled over $P_2O_5$ and stored over activated molecular sieves in a $N_2$ glovebox.

**Differential Scanning Calorimetry (DSC).** DSC was performed on 3.96 mg of M1 solid using instrument model DSC 822$^e$ from Mettler-Toledo GmbH Analytical. Samples were sealed in a standard aluminum crucible (ME-00027331) and underwent heating and cooling cycles between 25 and 140 °C. The first cycle started at 25 °C, heated from 25–140 at 2 °C/min, stayed at 140 °C for 5 min, cooled from 140–25 at 2 °C/min, stayed at 25 °C for 5 min, and then the cycle was repeated. Four total cycles were recorded.

**Device Fabrication.** Experimental conditions such as film thickness, annealing times, M1 concentration, M2 concentration, and solvent composition were optimized. Prepatterned indium-doped tin oxide (ITO) on glass was used as the transparent bottom electrode. The ITO was scrubbed with soapy water and cleaned by ultrasonicating sequentially in hexanes, soapy water, water, and a 1:1:1 solution of acetone/methanol/2-propanol. The electrode was then blown dry in a $N_2$ stream. The ITO surface was cleaned by UV-ozone treatment, and a thin film of PEDOT:PSS (Clevios P VP Al 4083) was immediately spin-cast on top. The PEDOT:PSS film was dried at 120 °C for 20 min and transferred into a $N_2$ glovebox ($O_2$ and $H_2O$ < 0.1 ppm). Bulk heterojunction photovoltaic devices were fabricated from a blend of a hairpin-shaped sexithiophene organogelator (M1) and either phenyl-$C_{61}$-butyric acid methyl ester (PCBM) or phenyl-$C_{71}$-butyric acid methyl ester ($PC_{71}BM$). Solutions of 5 mg/mL M1 and 27 mg/mL PCBM were filtered separately through 0.22 $\mu$m porous polytetrafluoroethylene filters and then mixed together in different ratios in either chlorobenzene or toluene. The blends were stirred at 60 °C in the glovebox for 12 h to ensure sufficient mixing. Films were cast by spin-coating at various speeds in the glovebox for 60 s. Total organic layer thicknesses ranged from 70 to 80 nm as determined by cross-sectional scanning electron microscopy. Devices were completed by thermally evaporating 6 Å of LiF then 100 nm of Al through a shadow mask at $1 \times 10^{-6}$ mbar to yield devices 4 mm$^2$ in area and sealed with a UV-curable epoxy. Fabricated and sealed devices were thermally annealed on a hot plate at various temperatures for 2 min and cooled to room temperature within a glovebox.

**Device Measurements.** Two-terminal measurements were performed using a Keithley 2400 source meter. Photovoltaic measurements were done while the devices were illuminated by an Oriel Xe solar simulator equipped with an Oriel 130 monochromator. Filters were used to cut off grating overtones. The solar spectrum was simulated using an AM1.5 filter with 80 mW/cm$^2$ power density. A calibrated silicon reference solar cell with a KG5 filter certified by the National Renewable Energy Laboratory was used to confirm the measurement conditions.

**Scanning Electron Microscopy (SEM).** Cross-sectional SEM micrographs were collected on a Hitachi field emission scanning electron microscope S4800 and LEO 1525 field emission scanning electron microscope. A 3 kV accelerating voltage was used with a secondary electron detector. Devices were scored on the back with a diamond-tipped scribe and fractured. Cross sections of fractured films were imaged without additional metal coatings.

**Atomic Force Microscopy (AFM).** Glass slides were cleaned and coated with PEDOT:PSS as described for device fabrication above. Blends of oligothiophene and fullerenes were spin-cast at various speeds in the glovebox for 60 s. AFM experiments were performed immediately following sample preparation and were recorded under ambient conditions on a multimode scanning probe microscope from Digital Instruments. The prepared films were also thermally annealed at the temperature that led to the highest device efficiency and imaged by AFM. Tapping-mode AFM was chosen to determine the morphology in order to minimize shear forces that cause distortion of the nanostructures and inaccuracy of the topology. Silicon cantilevers purchased from Asylum Research (AC240TS) were used in all AFM experiments.

**UV–Visible Spectroscopy (UV–Vis).** Transmission spectroscopy was collected on a PerkinElmer Lambda 1050 spectrophotometer on sealed devices before and after annealing using sealed substrates without active layers as a background.

**Fluorescence Titration Experiments.** Fluorescence spectroscopy was performed on an ISS PC1 photon counting fluorometer. All emission spectra were collected at a 90° angle. A quartz cell of 1 cm × 1 cm was used to hold 250 μL of 0.2 wt % (~1 mM) M1 solution in toluene. Small amounts of PCBM solution (30 mM) were added in 1 or 5 μL increments into the M1 solution, stirred, and equilibrated for 10 min before each measurement.

*Conflict of Interest:* The authors declare no competing financial interest.

*Acknowledgment.* This work was supported by the U.S. Department of Energy, Office of Science, Office of Basic Energy Sciences (DE-FG02-00ER45810) as well as support for L.C.P. from the National Science Foundation (DMR-0605427). This work also made use of the Nanoscale Integrated Fabrication, Testing and Instrumentation Center (NIFTI) for AFM, the Electron Probe Instrumentation Center (EPIC) for SEM and the Keck Biophysics Facility for the UV−vis spectrophotometer and fluorometer at Northwestern University. We thank S. Loser and I. Murray from Prof. T. Marks's research lab for their help in device fabrication.

*Supporting Information Available:* Complete fluorescence discussion, DSC, additional *J*−*V* curves, AFM, and additional optical data. This material is available free of charge *via* the Internet at http://pubs.acs.org.

## REFERENCES AND NOTES

1. Peet, J.; Heeger, A. J.; Bazan, G. C. "Plastic" Solar Cells: Self-Assembly of Bulk Heterojunction Nanomaterials by Spontaneous Phase Separation. *Acc. Chem. Res.* **2009**, *42*, 1700–1708.
2. Li, G.; Shrotriya, V.; Huang, J. S.; Yao, Y.; Moriarty, T.; Emery, K.; Yang, Y. High-Efficiency Solution Processable Polymer Photovoltaic Cells by Self-Organization of Polymer Blends. *Nat. Mater.* **2005**, *4*, 864–868.
3. Chen, H. Y.; Hou, J. H.; Zhang, S. Q.; Liang, Y. Y.; Yang, G. W.; Yang, Y.; Yu, L. P.; Wu, Y.; Li, G. Polymer Solar Cells with Enhanced Open-Circuit Voltage and Efficiency. *Nat. Photonics* **2009**, *3*, 649–653.
4. Park, S. H.; Roy, A.; Beaupre, S.; Cho, S.; Coates, N.; Moon, J. S.; Moses, D.; Leclerc, M.; Lee, K.; Heeger, A. J. Bulk Heterojunction Solar Cells with Internal Quantum Efficiency Approaching 100%. *Nat. Photonics* **2009**, *3*, 297–302.
5. Janssen, R. A. J.; Hummelen, J. C.; Saricifti, N. S. Polymer-Fullerene Bulk Heterojunction Solar Cells. *MRS Bull.* **2005**, *30*, 33–36.
6. Gunes, S.; Neugebauer, H.; Sariciftci, N. S. Conjugated Polymer-Based Organic Solar Cells. *Chem. Rev.* **2007**, *107*, 1324–1338.
7. Sirringhaus, H. Device Physics of Solution-Processed Organic Field-Effect Transistors. *Adv. Mater.* **2005**, *17*, 2411–2425.
8. Kim, Y.; Nelson, J.; Zhang, T.; Cook, S.; Durrant, J. R.; Kim, H.; Park, J.; Shin, M.; Nam, S.; Heeney, M.; McCulloch, I.; Ha, C. S.; Bradley, D. D. C. Distorted Asymmetric Cubic Nanostructure of Soluble Fullerene Crystals in Efficient Polymer: Fullerene Solar Cells. *ACS Nano* **2009**, *3*, 2557–2562.
9. Keawprajak, A.; Piyakulawat, P.; Klamchuen, A.; Iamraksa, P.; Asawapirom, U. Influence of Crystallizable Solvent on the Morphology and Performance of P3HT:PCBM Bulk-Heterojunction Solar Cells. *Sol. Energy Mater. Sol. Cells* **2010**, *94*, 531–536.
10. Zhao, J.; Swinnen, A.; Van Assche, G.; Manca, J.; Vanderzande, D.; Van Mele, B. Phase Diagram of P3HT/PCBM Blends and Its Implication for the Stability of Morphology. *J. Phys. Chem. B* **2009**, *113*, 1587–1591.
11. Miller, S.; Fanchini, G.; Lin, Y. Y.; Li, C.; Chen, C. W.; Su, W. F.; Chhowalla, M. Investigation of Nanoscale Morphological Changes in Organic Photovoltaics during Solvent Vapor Annealing. *J. Mater. Chem.* **2008**, *18*, 306–312.
12. Li, G.; Yao, Y.; Yang, H.; Shrotriya, V.; Yang, G.; Yang, Y. "Solvent Annealing" Effect in Polymer Solar Cells Based on Poly(3-hexylthiophene) and Methanofullerenes. *Adv. Funct. Mater.* **2007**, *17*, 1636–1644.
13. Walker, B.; Tomayo, A. B.; Dang, X. D.; Zalar, P.; Seo, J. H.; Garcia, A.; Tantiwiwat, M.; Nguyen, T. Q. Nanoscale Phase Separation and High Photovoltaic Efficiency in Solution-Processed, Small-Molecule Bulk Heterojunction Solar Cells. *Adv. Funct. Mater.* **2009**, *19*, 3063–3069.
14. Mayerhoffer, U.; Deing, K.; Gruss, K.; Braunschweig, H.; Meerholz, K.; Wurthner, F. Outstanding Short-Circuit Currents in BHJ Solar Cells Based on NIR-Absorbing Acceptor-Substituted Squaraines. *Angew. Chem., Int. Ed.* **2009**, *48*, 8776–8779.
15. Burckstummer, H.; Kronenberg, N. M.; Gsanger, M.; Stolte, M.; Meerholz, K.; Wurthner, F. Tailored Merocyanine Dyes for Solution-Processed BHJ Solar Cells. *J. Mater. Chem.* **2010**, *20*, 240–243.
16. Tamayo, A. B.; Walker, B.; Nguyen, T. Q. A Low Band Gap, Solution Processable Oligothiophene with a Diketopyrrolopyrrole Core for Use in Organic Solar Cells. *J. Phys. Chem. C* **2008**, *112*, 11545–11551.
17. Ma, B. W.; Woo, C. H.; Miyamoto, Y.; Frechet, J. M. J. Solution Processing of a Small Molecule, Subnaphthalocyanine, for Efficient Organic Photovoltaic Cells. *Chem. Mater.* **2009**, *21*, 1413–1417.
18. Loser, S.; Bruns, C. J.; Miyauchi, H.; Ortiz, R. P.; Facchetti, A.; Stupp, S. I.; Marks, T. J. A Naphthodithiophene-Diketopyrrolopyrrole Donor Molecule for Efficient Solution-Processed Solar Cells. *J. Am. Chem. Soc.* **2011**, *133*, 8142–8145.
19. Palmer, L. C.; Stupp, S. I. Molecular Self-Assembly into One-Dimensional Nanostructures. *Acc. Chem. Res.* **2008**, *41*, 1674–1684.
20. Hulvat, J. F.; Sofos, M.; Tajima, K.; Stupp, S. I. Self-Assembly and Luminescence of Oligo(*p*-phenylene vinylene) Amphiphiles. *J. Am. Chem. Soc.* **2005**, *127*, 366–372.
21. Messmore, B. W.; Hulvat, J. F.; Sone, E. D.; Stupp, S. I. Synthesis, Self-Assembly, and Characterization of Supramolecular Polymers from Electroactive Dendron Rodcoil Molecules. *J. Am. Chem. Soc.* **2004**, *126*, 14452–14458.
22. Stone, D. A.; Hsu, L.; Stupp, S. I. Self-Assembling Quinquethiophene-Oligopeptide Hydrogelators. *Soft Matter* **2009**, *5*, 1990–1993.
23. Tsai, W. W.; Li, L. S.; Cui, H. G.; Jiang, H. Z.; Stupp, S. I. Self-Assembly of Amphiphiles with Terthiophene and Tripeptide Segments into Helical Nanostructures. *Tetrahedron* **2008**, *64*, 8504–8514.
24. Stone, D. A.; Tayi, A. S.; Goldberger, J. E.; Palmer, L. C.; Stupp, S. I. Self-Assembly and Conductivity of Hydrogen-Bonded Oligothiophene Nanofiber Networks. *Chem. Commun.* **2011**, *47*, 5702–5704.
25. Pratihar, P.; Ghosh, S.; Stepanenko, V.; Patwardhan, S.; Grozema, F. C.; Siebbeles, L. D. A.; Wurthner, F. Self-Assembly and Semiconductivity of an Oligothiophene Supergelator. *Beilstein J. Org. Chem.* **2010**, *6*, 1070–1078.
26. Puigmarti-Luis, J.; Laukhin, V.; del Pino, A. P.; Vidal-Gancedo, J.; Rovira, C.; Laukhina, E.; Amabilino, D. B. Supramolecular Conducting Nanowires from Organogels. *Angew. Chem., Int. Ed.* **2007**, *46*, 238–241.
27. Sofos, M.; Stone, D. A.; Goswami, D. K.; Okasinski, J. S.; Jin, H.; Bedzyk, M. J.; Stupp, S. I. Nanoscale Structure of Self-Assembling Hybrid Materials of Inorganic and Electronically Active Organic Phases. *J. Phys. Chem. C* **2008**, *112*, 2881–2887.
28. Tajima, K.; Li, L. S.; Stupp, S. I. Nanostructured Oligo(*p*-phenylene vinylene)/Silicate Hybrid Films: One-Step Fabrication and Energy Transfer Studies. *J. Am. Chem. Soc.* **2006**, *128*, 5488–5495.
29. Xue, P. C.; Lu, R.; Zhao, L.; Xu, D. F.; Zhang, X. F.; Li, K. C.; Song, Z. G.; Yang, X. C.; Takafuji, M.; Ihara, H. Hybrid Self-Assembly of a π Gelator and Fullerene Derivative with Photoinduced Electron Transfer for Photocurrent Generation. *Langmuir* **2010**, *26*, 6669–6675.
30. Amabilino, D. B.; Puigmarti-Luis, J. Gels as a Soft Matter Route to Conducting Nanostructured Organic and Composite Materials. *Soft Matter* **2010**, *6*, 1605–1612.
31. Bushey, M. L.; Nguyen, T. Q.; Zhang, W.; Horoszewski, D.; Nuckolls, C. Using Hydrogen Bonds To Direct the Assembly of Crowded Aromatics. *Angew. Chem., Int. Ed.* **2004**, *43*, 5446–5453.

32. Canas-Ventura, M. E.; Xiao, W.; Wasserfallen, D.; Mullen, K.; Brune, H.; Barth, J. V.; Fasel, R. Self-Assembly of Periodic Bicomponent Wires and Ribbons. *Angew. Chem., Int. Ed.* **2007**, *46*, 1814–1818.
33. Schenning, A.; Meijer, E. W. Supramolecular Electronics; Nanowires from Self-Assembled $\pi$-Conjugated Systems. *Chem. Commun.* **2005**, 3245–3258.
34. Hoeben, F. J. M.; Jonkheijm, P.; Meijer, E. W.; Schenning, A. About Supramolecular Assemblies of $\pi$-Conjugated Systems. *Chem. Rev.* **2005**, *105*, 1491–1546.
35. Schenning, A.; Jonkheijm, P.; Peeters, E.; Meijer, E. W. Hierarchical Order in Supramolecular Assemblies of Hydrogen-Bonded Oligo(*p*-phenylene vinylene)s. *J. Am. Chem. Soc.* **2001**, *123*, 409–416.
36. Yamaguchi, T.; Ishii, N.; Tashiro, K.; Aida, T. Supramolecular Peapods Composed of a Metalloporphyrin Nanotube and Fullerenes. *J. Am. Chem. Soc.* **2003**, *125*, 13934–13935.
37. Jang, W. D.; Jiang, D. L.; Aida, T. Dendritic Physical Gel: Hierarchical Self-Organization of a Peptide-Core Dendrimer To Form a Micrometer-Scale Fibrous Assembly. *J. Am. Chem. Soc.* **2000**, *122*, 3232–3233.
38. Schillinger, E. K.; Mena-Osteritz, E.; Hentschel, J.; Borner, H. G.; Bauerle, P. Oligothiophene *versus* $\beta$-Sheet Peptide: Synthesis and Self-Assembly of an Organic Semiconductor-Peptide Hybrid. *Adv. Mater.* **2009**, *21*, 1562–1567.
39. Ajayaghosh, A.; Praveen, V. K. $\pi$-Organogels of Self-Assembled *p*-Phenylenevinylenes: Soft Materials with Distinct Size, Shape, and Functions. *Acc. Chem. Res.* **2007**, *40*, 644–656.
40. Ghosh, S.; Li, X. Q.; Stepanenko, V.; Wurthner, F. Control of H- and J-Type $\pi$ Stacking by Peripheral Alkyl Chains and Self-Sorting Phenomena in Perylene Bisimide Homo- and Heteroaggregates. *Chem.—Eur. J.* **2008**, *14*, 11343–11357.
41. Schoonbeek, F. S.; van Esch, J. H.; Wegewijs, B.; Rep, D. B. A.; de Haas, M. P.; Klapwijk, T. M.; Kellogg, R. M.; Feringa, B. L. Efficient Intermolecular Charge Transport in Self-Assembled Fibers of Mono- and Bithiophene Bisurea Compounds. *Angew. Chem., Int. Ed.* **1999**, *38*, 1393–1397.
42. Yagai, S.; Kinoshita, T.; Kikkawa, Y.; Karatsu, T.; Kitamura, A.; Honsho, Y.; Seki, S. Interconvertible Oligothiophene Nanorods and Nanotapes with High Charge-Carrier Mobilities. *Chem.—Eur. J.* **2009**, *15*, 9320–9324.
43. van Herrikhuyzen, J.; Syamakumari, A.; Schenning, A. P. H. J.; Meijer, E. W. Synthesis of n-Type Perylene Bisimide Derivatives and Their Orthogonal Self-Assembly with p-Type Oligo(*p*-phenylene vinylene)s. *J. Am. Chem. Soc.* **2004**, *126*, 10021–10027.
44. Ajayaghosh, A.; George, S. J.; Schenning, A. P. H. J. Hydrogen-Bonded Assemblies of Dyes and Extended $\pi$-Conjugated Systems. *Top. Curr. Chem.* **2005**, *258*, 83–118.
45. Gesquiere, A.; De Feyter, S.; De Schryver, F. C.; Schoonbeek, F.; van Esch, J.; Kellogg, R. M.; Feringa, B. L. Supramolecular $\pi$-Stacked Assemblies of Bis(urea)-Substituted Thiophene Derivatives and Their Electronic Properties Probed with Scanning Tunneling Microscopy and Scanning Tunneling Spectroscopy. *Nano Lett.* **2001**, *1*, 201–206.
46. Li, Y.; Li, G. T.; Wang, X. Y.; Li, W. N.; Su, Z. X.; Zhang, Y. H.; Ju, Y. Unique Twisted Ribbons Generated by Self-Assembly of Oligo(*p*-phenylene ethylene) Bearing Dimeric Bile Acid Pendant Groups. *Chem.—Eur. J.* **2009**, *15*, 6399–6407.
47. Prasanthkumar, S.; Gopal, A.; Ajayaghosh, A. Self-Assembly of Thienylenevinylene Molecular Wires to Semiconducting Gels with Doped Metallic Conductivity. *J. Am. Chem. Soc.* **2010**, *132*, 13206–13207.
48. Prasanthkumar, S.; Saeki, A.; Seki, S.; Ajayaghosh, A. Solution Phase Epitaxial Self-Assembly and High Charge-Carrier Mobility Nanofibers of Semiconducting Molecular Gelators. *J. Am. Chem. Soc.* **2010**, *132*, 8866–8867.
49. Wicklein, A.; Ghosh, S.; Sommer, M.; Wurthner, F.; Thelakkat, M. Self-Assembly of Semiconductor Organogelator Nanowires for Photoinduced Charge Separation. *ACS Nano* **2009**, *3*, 1107–1114.
50. Messmore, B. W.; Stupp, S. I. Mirror Image Nanostructures. *J. Am. Chem. Soc.* **2005**, *127*, 7992–7993.
51. Tsai, W.-W.; Tevis, I. D.; Tayi, A. S.; Cui, H.; Stupp, S. I. Semiconducting Nanowires from Hairpin-Shaped Self-Assembling Sexithiophenes. *J. Phys. Chem. B* **2010**, *114*, 14778–14786.
52. Coropceanu, V.; Cornil, J.; da Silva, D. A.; Olivier, Y.; Silbey, R.; Bredas, J. L. Charge Transport in Organic Semiconductors. *Chem. Rev.* **2007**, *107*, 926–952.
53. Yang, X. N.; Loos, J.; Veenstra, S. C.; Verhees, W. J. H.; Wienk, M. M.; Kroon, J. M.; Michels, M. A. J.; Janssen, R. A. J. Nanoscale Morphology of High-Performance Polymer Solar Cells. *Nano Lett.* **2005**, *5*, 579–583.
54. Padinger, F.; Rittberger, R. S.; Sariciftci, N. S. Effects of Postproduction Treatment on Plastic Solar Cells. *Adv. Funct. Mater.* **2003**, *13*, 85–88.
55. Kim, H. J.; Park, J. H.; Lee, H. H.; Lee, D. R.; Kim, J. J. The Effect of Al Electrodes on the Nanostructure of Poly(3-hexylthiophene): Fullerene Solar Cell Blends during Thermal Annealing. *Org. Electron.* **2009**, *10*, 1505–1510.
56. Clarke, T. M.; Ballantyne, A. M.; Nelson, J.; Bradley, D. D. C.; Durrant, J. R. Free Energy Control of Charge Photogeneration in Polythiophene/Fullerene Solar Cells: The Influence of Thermal Annealing on P3HT/PCBM Blends. *Adv. Funct. Mater.* **2008**, *18*, 4029–4035.
57. Mihailetchi, V. D.; Xie, H.; de Boer, B.; Koster, L. J. A.; Blom, P. W. M. Charge Transport and Photocurrent Generation in Poly(3-hexylthiophene):Methanofullerene Bulk-Heterojunction Solar Cells. *Adv. Funct. Mater.* **2006**, *16*, 699–708.
58. Muller, C.; Ferenczi, T. A. M.; Campoy-Quiles, M.; Frost, J. M.; Bradley, D. D. C.; Smith, P.; Stingelin-Stutzmann, N.; Nelson, J. Binary Organic Photovoltaic Blends: A Simple Rationale for Optimum Compositions. *Adv. Mater.* **2008**, *20*, 3510–3515.
59. Muck-Lichtenfeld, C.; Grimme, S.; Kobryn, L.; Sygula, A. Inclusion Complexes of Buckycatcher with $C_{60}$ and $C_{70}$. *Phys. Chem. Chem. Phys.* **2010**, *12*, 7091–7097.
60. Perez, E. M.; Martin, N. Molecular Tweezers for Fullerenes. *Pure Appl. Chem.* **2010**, *82*, 523–533.